Korean J. Chem. Eng., 37(6), 1066-1070 (2020)
DOI: 10.1007/s11814-020-0490-9

pISSN: 0256-1115
eISSN: 1975-7220

Investigation on the performance of SnS solar cells grown by sputtering and effusion cell evaporation

Dong-seob Jeong‡, Vasudeva Reddy Minnam Reddy‡, Mohan Reddy Pallavolu‡, Haeyun Cho, and Chinho Park†

School of Chemical Engineering, Yeungnam University, 280 Daehak-ro, Gyeongsan 38541, Korea
(*Received 17 September 2019 • accepted 9 January 2020*)

Abstract−SnS is an earth-abundant, non-toxic, and low-cost absorber material for solar cell applications. In this work, the physical properties of SnS thin films and efficiency of SnS solar cells were investigated for different tin metal layer thicknesses of 300 nm (Sn-300), 500 nm (Sn-500), and 700 nm (Sn-700) deposited by DC sputtering followed by the sulfurization using effusion cell evaporation method. The XRD and Raman characterizations confirmed the formation of single-phase SnS compound with orthorhombic structure for the case of Sn-500. The sulfurized films of Sn-500 had remarkable and homogeneous morphology with the optical band gap energy of 1.35 eV. The fabricated device showed an efficiency of 0.74% with an open-circuit voltage of 267 mV, short circuit current density of 8.47 mA/cm^2, and fill factor of 54.16. By varying the different metal tin layer thicknesses, this is the first report with device efficiency for SnS solar cells grown via effusion cell evaporation technique.

Keywords: SnS Solar Cells, Physical Properties, SnS Compound, Metal Tin Layer Thickness

INTRODUCTION

Due to the rapid increase of energy demand annually, the present generation desires electrical power at lower cost and inexpensive root without affecting the environment. Only solar power is the ultimate source for the production of clean energy at lower cost. Over the decades, many studies have reported on different solar power generated materials. Particularly, thin film solar cells based on the binary compound are promising compared to the ternary and quaternary compound based solar cells. Among the binary compounds, Sn-based compound (SnS) has great potential due to its capable optoelectronic properties. SnS has an optical bandgap of 1.0-1.5 eV, high absorption coefficient, p-type conductivity, and considerably high carrier mobility [1-4]. Even though the SnS has exhibited promising properties, lower efficiencies have been displayed due to the secondary phases and many defects in the absorber layer [5].

Defects can be lowered by maneuvering the fabrication processes. Specifically, in the industrial two-stage process, the growth of SnS films can be controlled carefully. The two-stage process involves deposition of Sn by a physical technique followed by sulfurization. In the first stage, metallic Sn layer deposition is performed by a physical method such as sputtering and evaporation, because the physical methods can yield higher reproducibility of thin films than the chemical methods. In the second stage, compound formation is controlled by the sulfurization process using rapid thermal processing (RTP) or effusion cell process, which plays crucial role in defect-free compound formation. Effusion cell evaporation is an efficient and controllable deposition technique with excellent incorporation characteristics of sulfur source. It has precise controllability of temperature with great advantage and thus has been widely used in molecular beam epitaxial deposition systems [6,7] with a wide range of sizes. Most of the studies on SnS solar cells involve the effect of different temperatures [8,9], different compositional ratios [10], different annealing conditions [11], different pressure variations [12,13], etc., but there is no approach to different metal layer thickness variation that influences the diffusion of sulfur into tin and physical properties of SnS. Tin metal thickness majorly influences the sulfurization reaction process between tin and sulfur, as high metal tin cannot react well with sulfur that causes to form secondary phases or unreacted metal may present in the film, which is based on the diffusion length of sulfur into the tin. Therefore, there is a need to optimize the tin metal layer thickness for good reaction of tin with sulfur.

Therefore, in the present investigation, SnS solar cells were fabricated by a two-stage process (sputtering and effusion cell evaporation), and the absorber layer deposition was carried out by varying the tin metallic layer thicknesses. Based on the preparation conditions, SnS compound can be obtained by the reaction between tin and sulfur, with the appearance of secondary phases of SnS_2 and Sn_2S_3 [14]. The thickness of tin layers plays a decisive role in the diffusion of sulfur and the formation of single-phase SnS compound with decent morphology. The present results showed the best device efficiency of 0.74% in the case of SnS formed using Sn-500.

EXPERIMENTAL DETAILS

1. SnS Absorber Layer Formation

The fabrication of SnS solar cells by a two-stage process involves the following: metal layer deposition is carried out in the first stage and the sulfurization process in the second stage. Before deposit-

†To whom correspondence should be addressed.
E-mail: chpark@ynu.ac.kr
‡Authors have equal contribution

ing tin metal layer, the soda-lime glass (SLG) substrates and molybdenum coated glass substrates were cleaned in acetone, methanol, and deionized water, respectively, with required times under ultrasonication. The 99.99% purity Sn target was used for the deposition of metallic tin layers by a sputtering system. The deposition conditions of sputtering for metallic tin are as follows: sputtering chamber was evacuated to 3×10^{-6} Torr (base pressure), working pressure of 5 mTorr, and DC power of 150 W in an argon atmosphere with 40 sccm flow rate. By varying the sputter deposition time, the tin layer thickness can be varied. Further, the deposited tin metallic precursors with different thicknesses of 300 nm (Sn-300), 500 nm (Sn-500), and 700 nm (Sn-700) were inserted into the effusion cell evaporation system with 5 g of sulfur flakes for sulfurization. The distance between substrate rotator and the sulfur source was around 45 cm. The effusion cell evaporation system was evacuated to 5×10^{-5} Torr and then pumped with N_2 gas flow during the deposition process to maintain the working pressure of 5 mTorr. The SnS thin films were prepared for different tin precursor film thicknesses with substrate temperature of 470 °C and sulfur source temperature of 170 °C. After completion of SnS film formation, the system was then cooled to room temperature naturally.

2. SnS Solar Cell Fabrication

SnS thin film solar cells with the structure of SLG/Mo/SnS/CdS/i-ZnO/Al:ZnO/Ni/Ag were fabricated. The deposited SnS absorber films were placed in a distilled water flow for 10 min prior to the deposition of CdS buffer layer. The buffer layer was made by CBD technique using aqueous solutions of $CdSO_4$, $(NH_2)_2CS$, NH_4OH, and D. I. water. Cd source solution was prepared with the concentration of 0.0074 M cadmium sulfate $CdSO_4$ (99.0%, sigma Aldrich), sulfur source solution was prepared with the concentration of 0.2 M thiourea ($(NH_2)_2CS$, C.P, Duksan). Ammonia water (NH_4OH, Extra Pure GRADE, Duksan) was used as a complexing agent. Next, the substrates were vertically mounted on a holder and kept in the bath solution. The deposition was carried out at a bath temperature of 80 °C for 26 min. The buffer layer thickness was around 60 nm. The buffer layer deposited on SnS absorber films was then soaked for one hour at 200 °C. The deposition of window layers of ZnO was by a two-step magnetron sputtering: the first layer consisted of i-ZnO by radio-frequency (RF) sputtering, and the second layer consisted of Al-doped ZnO by DC magnetron sputtering. The thickness of i-ZnO layer was around 50 nm, and the Al-doped ZnO was around 350 nm. Ni and Ag top contacts were deposited by electron beam evaporation with the thicknesses of 50 nm and 500 nm, respectively. Finally, the SnS films were scribed and the device efficiency was measured for the active area of 0.4 cm^2.

3. Characterization

Using powder X-ray diffractometer, the SnS films were characterized for crystallographic structure analysis. An X-ray diffractometer (Bulk PANalytical X' Pert-PRO multipurpose diffractometer (MPD), 3 kW) with Cu Kα radiation of wavelength 0.1546 nm at 40 kV and 30 mA was used for recording the XRD data. Raman spectrometer (Model: HORIBA Xplora Plus) was used for the phase analysis of SnS films, and the spectra were recorded in the range of 50-500 cm^{-1} using 532 nm laser source. The morphological and cross-sectional view of images for SnS films were characterized by field emission scanning electron microscopy (FE-SEM, HITACHI, S-4800). Diffuse reflectance spectra of SnS films were recorded by UV-Vis-NIR double beam spectrophotometer (Cary 5000) in the wavelength range of 300-1,500 nm. The SnS solar cell device characteristics were measured using a Xenon flash lamp (USHIO, UA-DF1, 100 mW/cm^2, 400 V) by the Keithley 2400 with AM1.5 filter. The devices were characterized for spectral response using external quantum efficiency (EQE) measurement system to evaluate the photovoltaic response.

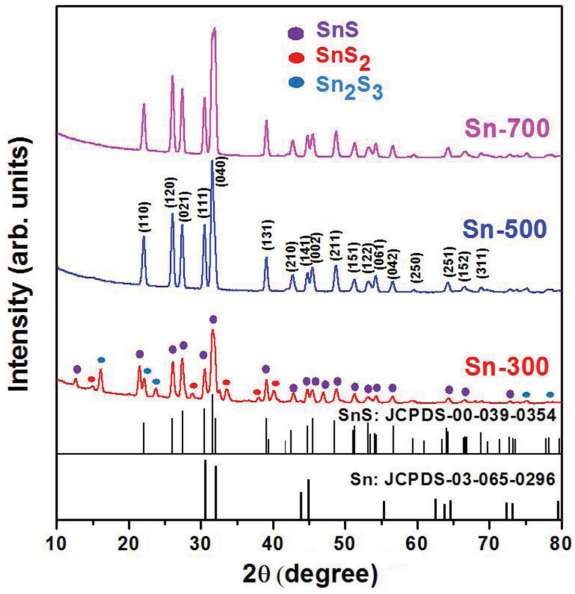

Fig. 1. XRD patterns of SnS films prepared for different thicknesses of tin metal layer.

RESULTS AND DISCUSSION

1. Crystallographic Analysis

The characterized XRD patterns of SnS films are shown in Fig. 1. From the XRD patterns of the SnS films, it is noticed that all the films are in polycrystalline nature with (040) sharp intense peak as preferred orientation. The sulfurized film of Sn-300 shows peaks at 22.01°, 26.01°, 27.47°, 31.53°, 31.97°, 39.04°, 42.50°, 44.74°, 45.49°, 48.51°, 51.31°, 53.14°, 54.25°, 56.67°, 59.34°, 64.19°, 66.37°, and 69.76° which correspond to (110), (120), (021), (111), (040), (131), (210), (141), (002), (211), (151), (122), (061), (042), (250), (251), (152), and (311) planes of orthorhombic SnS (JCPDS: 00-039-0354) [15], respectively, in addition to some Sn_2S_3 and SnS_2 secondary phase peaks. Additional peaks of Sn_2S_3 and SnS_2 peaks were observed due to presumably too low thickness of metallic tin. This means that Sn-300 layer was not sufficient for the formation of SnS compound without secondary phases at this deposition condition. The sulfur incorporation into the tin leads to the formation of SnS single phase during the sulfurization process [13]. On the other hand, sulfurized films of Sn-500 show high and sharp intense peaks of SnS only due to the sufficient metallic tin layer thickness. However, further, an increase in precursor metal thickness to 700 nm, the unreacted Sn layer was present in the sulfurized films. The intensity of the preferred orientation peak as well as other peaks related

to SnS was increased with increase of tin thickness from 300 nm to 500 nm but decreased at larger thickness of 700 nm. As can be noticed from Fig. 1, the XRD patterns of Sn and SnS peaks appeared on the thicker film and no other peaks related to Sn_2S_3 and SnS_2 were observed. According to the diffraction profiles and as evidenced by Robles et al.'s XRD results, the mixed phases of Sn and SnS appeared to the thicker film [16]. Moreover, the standard JCPDS lines of Sn and SnS are shown at the same place; assessment of phase formation by XRD alone is very difficult. This means that an excess of metal tin was present in the film that cannot be sulfurized at this condition due to the high thickness of metallic tin layer. The presence of SnS and Sn was also identified by Minemura et al. [9]. From the XRD results, the formation of SnS compound and other secondary phases were both observed with the change in precursor metal layer thickness, which indicates that metallic tin layer thickness influences significantly the formation of secondary phases, and single-phase SnS compound or metallic tin influences the stoichiometric deviation in the formation of SnS compound. The 500 nm thick metallic tin was sufficient in the formation of SnS compound at the deposition conditions used in this study. For a detailed investigation of structural properties, Raman analysis was performed.

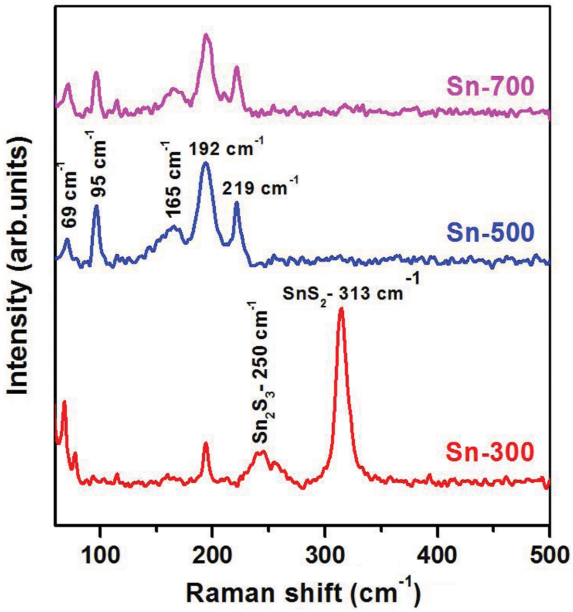

Fig. 2. Raman spectra of the SnS films deposited for different thicknesses of tin metal layer.

2. Raman Analysis

The Raman spectra of the deposited SnS films for different tin metal precursor layer thicknesses are shown in Fig. 2. The sulfurized film of Sn-300 shows high intense Raman mode at 313 cm^{-1} related to SnS_2 and 250 cm^{-1} related to Sn_2S_3 [17-19], in addition to SnS phases. The exhibited Raman modes of SnS_2 and Sn_2S_3 are due to the insufficient metallic tin. The sulfurized film of Sn-500 shows Raman modes at 69 cm^{-1}, 95 cm^{-1}, 165 cm^{-1}, 192 cm^{-1}, and 219 cm^{-1} that are related to orthorhombic-SnS [20] due to the availability of sufficient thick tin metal precursor. The exhibited Raman modes at 69 cm^{-1}, 95 cm^{-1}, 165 cm^{-1}, 192 cm^{-1}, and 219 cm^{-1} are in good agreement with the orthorhombic-SnS, and peaks were not observed above 300 cm^{-1} which confirmed the absence of secondary phases [21]. However, the film sulfurized for Sn-700 exhibited Raman modes belonging to SnS. Therefore, from the XRD and Raman studies, single phase SnS films can be deposited with Sn-500 in the effusion cell sulfurization method.

3. Morphology Analysis

Fig. 3 shows the surface view and inset with the cross-sectional view of FE-SEM images for the films sulfurized at different precursor metal tin layer thicknesses. The remarkable morphological SnS film can be developed by a sufficient tin metal precursor layer which reacts with sulfur. The grain size and thickness of the film increased with respect to thickness of tin layers. In the present case, the sulfurized film for Sn-300 was not enough to produce good grain homogeneous morphology, because the lower thicknesses of tin were not sufficient for reaction with sulfur vapor pressure that causes to generate secondary phases and big voids and/or pores. As can be observed from Fig. 3, the sulfurized film shows thickness of around 550 nm. The uniformly distributed flat-like homogeneous grain structures were obtained for Sn-500 sulfurized film. From the surface morphology of the SnS films was observed the variation of the grain structures related to the change in crystalline nature of the SnS XRD peaks [22]. After sulfurization, the grain size and thickness (from around 550 nm to 750 nm) of the film increased. When Sn-700 was used, the sulfurized film showed mixed grains of complex and uneven structure. The excess of tin cannot react with sulfur vapor pressure that causes to present unreacted metallic tin in the film, and these sulfurized films had a thickness

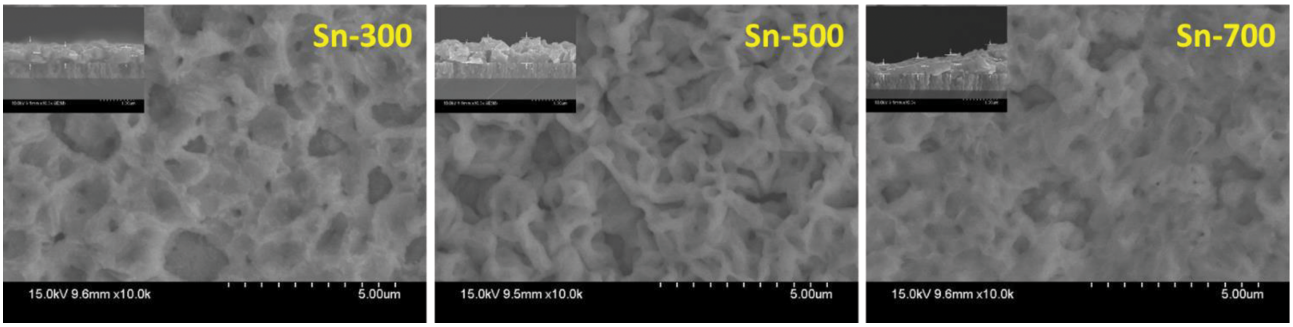

Fig. 3. Morphological FE-SEM images of SnS films deposited for different tin metal thicknesses inset with cross sectional images of sulfurized films.

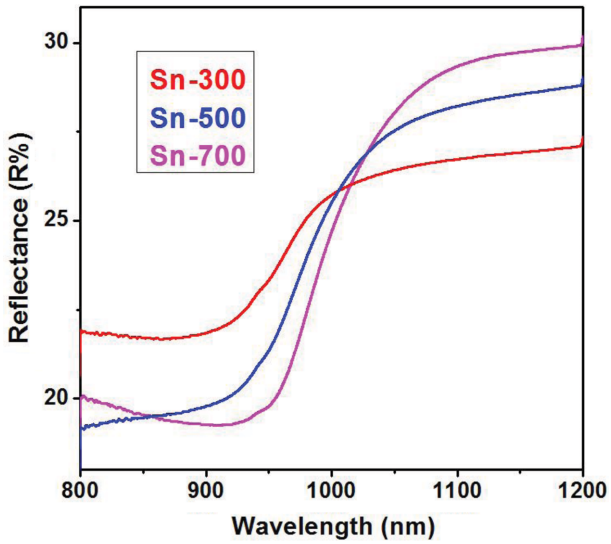

Fig. 4. Reflectance spectra of the SnS films deposited for different tin metal thicknesses.

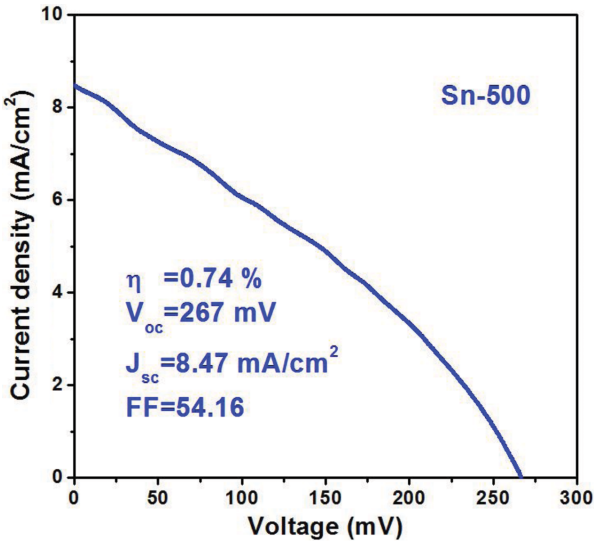

Fig. 5. Efficiency report of the SnS thin film sulfurized for Sn-500.

of around 900 nm. From the morphological studies, it is noticed that the tin metal precursor layer thickness can influence the morphology of the SnS films significantly, and sufficient metallic Sn can only develop a good grain structure by the reaction of metal tin with sufficient sulfur vapor pressure.

4. Optical Studies

Fig. 4 shows the optical reflectance spectra of the deposited SnS films for different metal precursor layer thicknesses. The reflectance spectra of the sulfurized film for Sn-700 show higher reflectance than that of the sulfurized films of Sn-300 and Sn-500, which is due presumably to the unreacted tin present in the film. With respect to the change of metal tin precursor layer thickness, the incorporation of sulfur into tin was well made, and then reflectance was also decreased due to the presence of unreacted Sn. As observed from the optical reflectance data, the sudden fall of reflectance edge was changed to lower side of wavelength range, which was due to the presence of secondary phases in the film that influences the bandgap.

From the diffuse reflectance data, the bandgap energy was calculated. The calculated bandgap of the SnS films varied in the range of 1.45-1.31 eV with respect to the change of metal tin precursor layer thickness. The film sulfurized for Sn-300 had a bandgap of 1.45 eV. The exhibited bandgap was greater than the remaining films exhibited bandgap, which was due to the presence of both SnS_2 and SnS_3 secondary phases or non-crystalline natured films which had lower thickness that led to the higher optical bandgap [23]. The obtained bandgap of 1.35 eV for Sn-500 sulfurized film matched well with the reported values for SnS films [2,24]. The decrease in optical bandgap is due to the suppression of secondary phases. However, the film grown for Sn-700 showed a lower bandgap of 1.31 eV due to the presence of tin. Based on the method of deposition, the bandgap was changed with respect to the deposition conditions.

5. Photovoltaic Performance of the SnS Solar Cells

Fig. 5 shows the illuminated J-V characteristics of SnS solar cell sulfurized at Sn-500. Among the three fabricated SnS solar cells, the best device performance was achieved for Sn-500 sulfurized film. The best device exhibited a short circuit current density of 8.47 mA/cm^2, open-circuit voltage of 267 mV, fill factor of 54.16, and the conversion efficiency of 0.74% under AM1.5. The remaining fabricated SnS solar cells did not show any efficiency because of the secondary phase effect or metallic tin present in those films. The high series resistance is the most significant problem to decrease the photovoltaic response in the device, which is caused by the buffer CdS layer [25]. The low J_{sc} is also one of the factors for lower efficiency in the present SnS solar cell device, which is due to the high charge carrier recombination at junctions as well as minority carrier lifetime [1]. The lower efficiencies are due to the more defects in the absorber or bad p-n junction formation. More considerable efforts are in progress to enhance the efficiency of SnS solar cells. To enhance the SnS solar cells efficiency, majorly,

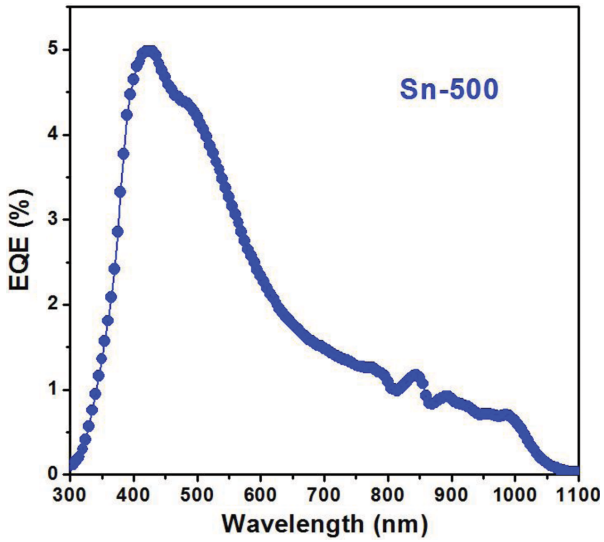

Fig. 6. EQE plot of the SnS thin film sulfurized for Sn-500.

high quality SnS absorber is required and the formation of the p-n junction at lower recombination rate must be achieved [26].

Fig. 6 shows the SnS/CdS device spectral response for SnS films sulfurized at Sn-500. As seen, the maximum quantum efficiency is around 50% and there is no spectral response for other sulfurized films. The EQE of SnS solar cell show relatively lower value above 800 nm due to the bulk recombination in SnS [3] and poor charge collection at the p-n junction. The onset absorption of SnS has a bandgap of 1.35 eV. The sharp drop at ~500 nm from Fig. 6 indicates the absorption edge of CdS (2.4 eV). In polycrystalline materials, the lower response of spectra at longer wavelengths indicates smaller values of minority carrier diffusion length. Increment or decrement of EQE response depends on the recombination rate by varying the defects concentration [27].

CONCLUSIONS

SnS solar cells were fabricated by sputtering followed with the effusion cell evaporation method. The physical properties of the sulfurized SnS films were investigated. XRD showed the formation of orthorhombic-SnS compound with (040) as preferred orientation peak. Raman modes of 69 cm^{-1}, 95 cm^{-1}, 165 cm^{-1}, 192 cm^{-1}, and 219 cm^{-1} confirmed the strong evidence of the formation of the orthorhombic-SnS compound. The film sulfurized for Sn-500 showed remarkable homogeneous morphology with the bandgap energy of 1.35 eV. The film sulfurized for Sn-500 showed the best device efficiency of 0.74% with an open-circuit voltage of 267 mV, short circuit current of 8.47 mA/cm^2, and fill factor of 54.16 under AM1.5. Our results motivate enhancing of SnS solar cell efficiency in the near future.

ACKNOWLEDGEMENTS

This study was supported by the Human Resources Program in Energy Technology of the Korea Institute of Energy Technology Evaluation and Planning (KETEP), granted financial resource from the Ministry of Trade, Industry & Energy, Republic of Korea (Grant No. 20154030200760).

REFERENCES

1. V. R. M. Reddy, S. Gedi, C. Park, R. W. Miles and K. T. R. Reddy, *Curr. Appl. Phys.*, **15**, 588 (2015).
2. S. Gedi, V. R. M. Reddy, C. Park, J. C. Wook and K. T. R. Reddy, *Opt. Mater.*, **42**, 468 (2015).
3. P. Sinsermsuksakul, J. Heo, W. Noh, A. S. Hock and R. G. Gordon, *Adv. Energy Mater.*, **1**, 1116 (2011).
4. G. Ham, S. Shin, J. Park, H. Choi, J. Kim, Y.-A. Lee, H. Seo and H. Jeon, *ACS Appl. Mater. Interfaces*, **5**, 8889 (2013).
5. A. Schneikart, H.-J. Schimper, A. Klein and W. Jaegermann, *J. Phys. Appl. Phys.*, **46**, 305109 (2013).
6. R. A. Kubiak, P. Driscoll and E. H. C. Parker, *J. Vac. Sci. Technol.*, **20**, 252 (1982).
7. H. F. Tiedje and D. E. Brodie, *Rev. Sci. Instrum.,* **71**, 2121 (2000).
8. R. Chakraborty, V. Steinmann, N. M. Mangan, R. E. Brandt, J. R. Poindexter, R. Jaramillo, J. P. Mailoa, K. Hartman, A. Polizzotti, C. Yang, R. G. Gordon and T. Buonassisi, *Appl. Phys. Lett.*, **106**, 203901 (2015).
9. T. Minemura, K. Miyauchi, K. Noguchi, K. Ohtsuka, H. Nakanishi and M. Sugiyama, *Phys. Status Solidi C*, **6**, 1221 (2009).
10. A. Yago, T. Kibishi, Y. Akaki, S. Nakamura, H. Oomae, H. Katagiri and H. Araki, *Jpn. J. Appl. Phys.*, **57**, 02CE08 (2018).
11. N. Revathi, S. Bereznev, M. Loorits, J. Raudoja, J. Lehner, J. Gurevits, R. Traksmaa, V. Mikli, E. Mellikov and O. Volobujeva, *J. Vac. Sci. Technol. Vac. Surf. Films*, **32**, 061506 (2014).
12. S. Mikami, T. Yokoi, H. Sumi, S. Aihara, I. Khatri and M. Sugiyama, *Phys. Status Solidi C*, **14**, 1600160 (2017).
13. R. Caballero, V. Condé and M. León, *Thin Solid Films*, **612**, 202 (2016).
14. T. Jiang and G. A. Ozin, *J. Mater. Chem.*, **8**, 1099 (1998).
15. J. Kim, J. Kim, S. Yoon, J. Kang, C.-W. Jeon and W. Jo, *J. Phys. Chem. C*, **122**, 3523 (2018).
16. V. Robles, J. F. Trigo, C. Guillén and J. Herrero, *Thin Solid Films*, **582**, 249 (2015).
17. H. R. Chandrasekhar and D. G. Mead, *Phys. Rev. B*, **19**, 932 (1979).
18. L. S. Price, I. P. Parkin, A. M. E. Hardy, R. J. H. Clark, T. G. Hibbert and K. C. Molloy, *Chem. Mater.*, **11**, 1792 (1999).
19. J. Chao, Z. Xie, X. Duan, Y. Dong, Z. Wang, J. Xu, B. Liang, B. Shan, J. Ye, D. Chen and G. Shen, *CrystEngComm*, **14**, 3163 (2012).
20. H. R. Chandrasekhar, R. G. Humphreys, U. Zwick and M. Cardona, *Phys. Rev. B*, **15**, 2177 (1977).
21. S. Di Mare, D. Menossi, A. Salavei, E. Artegiani, F. Piccinelli, A. Kumar, G. Mariotto and A. Romeo, *Coatings*, **7**, 34 (2017).
22. P. A. Nwofe, K. T. R. Reddy, J. K. Tan, I. Forbes and R. W. Miles, *J. Phys. Conf. Ser.*, **417**, 012039 (2013).
23. P. Pramanik, P. K. Basu and S. Biswas, *Thin Solid Films*, **150**, 269 (1987).
24. R. E. Banai, L. A. Burton, S. G. Choi, F. Hofherr, T. Sorgenfrei, A. Walsh, B. To, A. Cröll and J. R. S. Brownson, *J. Appl. Phys.*, **116**, 013511 (2014).
25. H. Li, S. Cheng, J. Zhang, W. Huang, H. Zhou and H. Jia, *World J. Condens. Matter Phys.*, **5**, 10 (2015).
26. J. A. A. Arvizu, M. C. Piedrahita and O. V. Glalan, *J. Mater. Sci. Mater. Electron.*, **26**, 4541 (2015).
27. V. Steinmann, R. Jaramillo, K. Hartman, R. Chakraborty, R. E. Brandt, J. R. Poindexter, Y. S. Lee, L. Sun, A. Polizzotti, H. H. Park, R. G. Gordon and T. Buonassisi, *Adv. Mater.*, **26**, 7488 (2014).